

# Discovery of a First-in-Class Inhibitor of the Histone Methyltransferase SETD2 Suitable for Preclinical Studies

Published as part of the ACS Medicinal Chemistry Letters special issue "Epigenetics 2022".

John W. Lampe, Joshua S. Alford, P. Ann Boriak-Sjodin, Dorothy Brach, Kat Cosmopoulos, Kenneth W. Duncan, Sean T. Eckley, Megan A. Foley, Darren M. Harvey, Vinny Motwani, Michael J. Munchhof, Alejandra Raimondi, Thomas V. Riera, Cuyue Tang, Michael J. Thomenius, Jennifer Totman, and Neil A. Farrow\*



Cite This: *ACS Med. Chem. Lett.* 2021, 12, 1539–1545



Read Online

ACCESS |



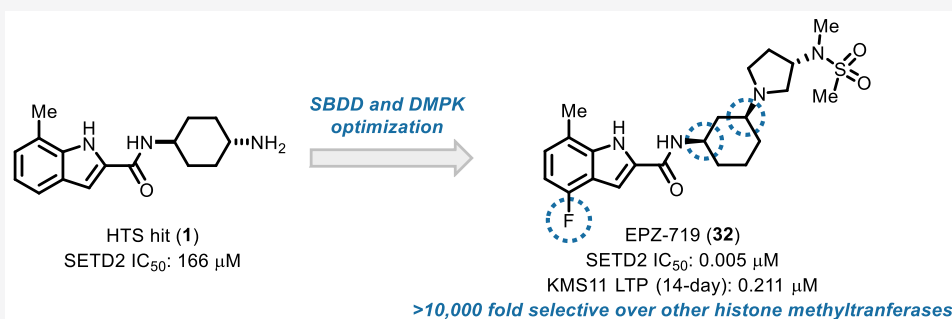
Metrics & More



Article Recommendations



Supporting Information



**ABSTRACT:** SET domain-containing protein 2 (SETD2), a histone methyltransferase, has been identified as a target of interest in certain hematological malignancies, including multiple myeloma. This account details the discovery of EPZ-719, a novel and potent SETD2 inhibitor with a high selectivity over other histone methyltransferases. A screening campaign of the Epizyme proprietary histone methyltransferase-biased library identified potential leads based on a 2-amidoindole core. Structure-based drug design (SBDD) and drug metabolism/pharmacokinetics (DMPK) optimization resulted in EPZ-719, an attractive tool compound for the interrogation of SETD2 biology that enables *in vivo* target validation studies.

**KEYWORDS:** Histone methyltransferase, SETD2

The lysine *N*-methyltransferase SETD2,<sup>1</sup> is the only known enzyme capable of the trimethylation of histone H3 lysine 36 (H3K36)<sup>2</sup> and has been reported to play a role in transcriptional elongation<sup>3,4</sup> and alternative splicing.<sup>5,6</sup> Although SETD2 has been shown to have a role as a tumor suppressor,<sup>7–10</sup> our target identification efforts identified it as a potential target of interest for the treatment of some cancers.<sup>11</sup> Inhibitors of SETD2 have been described in the literature;<sup>12</sup> however, none are suitable for *in vivo* studies. To further validate this target, we sought a suitable small molecule inhibitor that could be used to thoroughly interrogate SETD2 biology both *in vitro* and *in vivo*. Herein, we detail the efforts that led to the identification of a selective SETD2 inhibitor with these desirable properties.

The modulation of epigenetic targets with small molecules has been part of our strategy to understand the biology of various histone methyltransferases.<sup>13</sup> During the course of these efforts, we developed a histone methyltransferase-biased library enriched with chemotypes that possessed desirable physiochemical properties, which could be elaborated into tool compounds.

We screened our in-house library against SETD2 in a radiometric assay that monitored the methylation of a histone peptide and identified two hits of interest, compounds 1 and 2 (Figure 1).

Hits 1 and 2 were confirmed in the SETD2 biochemical assay with IC<sub>50</sub> values of 166 and 22.1 μM, respectively. Further workup in our hit validation funnel demonstrated that 1 and 2 were true hits. Both 1 and 2 show reversible inhibition of SETD2, with an uncompetitive mechanism with respect to the substrate *S*-adenosylmethionine (SAM) and a noncompetitive mechanism with respect to the peptide substrate. Further, compound 2 displayed well-behaved binding in a surface

Received: May 11, 2021

Accepted: August 16, 2021

Published: August 24, 2021



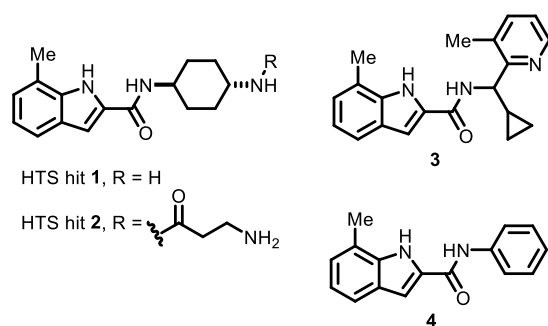


**Figure 1.** Initial screening hits and results of the initial optimization.

plasmon resonance (SPR) binding assay with a  $K_D$  value of 40  $\mu\text{M}$ , and we obtained a ligand-bound X-ray cocrystal structure at 2.30 Å between compound 2, SAM, and SETD2 (Figure 2).

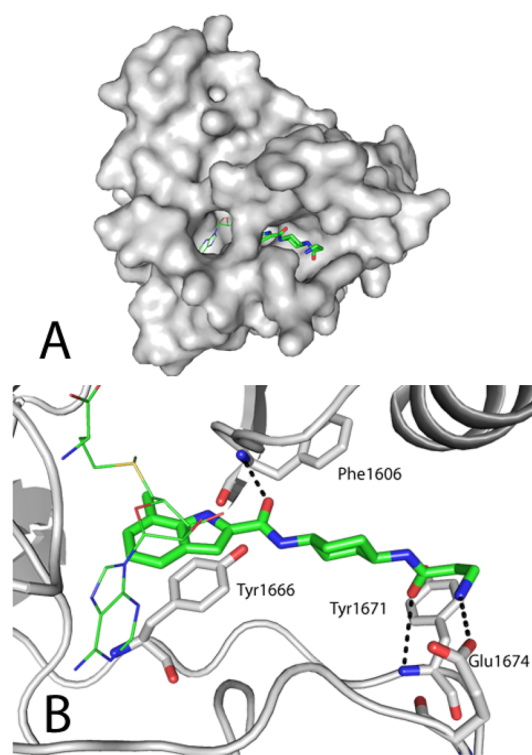


**Figure 2.** X-ray structure of HTS hit 2. Compound 2 is represented as sticks, and SAM is represented as lines. (A) Surface representation of SETD2 showing the location of compound 2 at right relative to the SAM binding site. (B) Binding mode of compound 2 showing key interactions with SETD2 and the proximity to the SAM binding site.

The structure of the ligand-bound complex shows that 2 occupies a portion of the enzyme's peptide binding site, with the 7-methylindole buried deep within the lysine channel where histone 3 lysine 36 would normally be positioned for methylation by SAM. In this binding pose, the indole aromatic rings make a face-to-face  $\pi$ -stacking interaction with Tyr1666. The indole N–H and the indolecarboxamide carbonyl interact with the backbone carbonyl and N–H from Phe1606, respectively, via H-bonding, and the cyclohexane ring of the ligand makes predominantly nonpolar contacts with the protein. The  $\beta$ -alanine terminus was poorly resolved, presumably due to its high degree of flexibility and mobility within the crystal lattice. Although the noncompetitive mechanism of 2 with

respect to the peptide substrate may seem at odds with the observed binding location in the X-ray structure, this type of relationship was observed previously<sup>14–16</sup> and may occur for a variety of reasons, such as exosite binding. Additional follow-up efforts led to the identification of compounds 3, with a biochemical  $\text{IC}_{50}$  value of 2.08  $\mu\text{M}$ , and 4, with a biochemical  $\text{IC}_{50}$  value of 4.24  $\mu\text{M}$ , as potential starting points for further elaboration.

To assess the importance of substitution at the 7-position of the indole, we utilized a small collection of compounds (Table 1) to assess the impact of this structural motif. We found that

**Table 1.** Effect of Indole Substitution and the Core Change

Cmpd	R	<sup>a</sup> SETD2 $\text{IC}_{50}$ ( $\mu\text{M}$ )	Cmpd	R	SETD2 $\text{IC}_{50}$ ( $\mu\text{M}$ )
3		2.08	10		>200
5		>200	11		>200
6		>200	12		>200
7		>200	13		>200
8		0.674	14		>50
9		5.46	15		>200

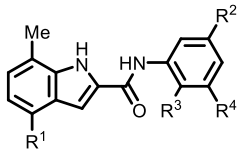
<sup>a</sup>Standard deviations for the active compounds are less than 13% of the  $\text{IC}_{50}$  values.

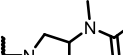
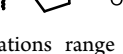
compounds containing the 7-methylindole displayed significant activity in the biochemical assay. Moreover, the X-ray structure of 2 showed that the indole was positioned deep within the lysine channel and was highly engaged with the protein, which was further validated by analogs that explored the structure–activity relationship (SAR) of the indole unit based on compound 3 (Table 1). In combination with this methyl, some substitution with fluorine was tolerated, as shown by 8 and 9, with substitution at the 4-position leading to significant improvements in the activity. The indole unit was generally tolerated better as compared to other heterocycles, which is consistent with the observed crystal structure. We therefore

focused our synthetic efforts on 7-methylindole- and 4-fluoro-7-methylindole-containing analogs.

Despite improvements in the biochemical potency for derivatives of compound **3** and our efforts to improve the physical and DMPK properties of the molecules, progressing this subseries remained difficult. We therefore refocused our optimization efforts on compound **4**. Our work in this new series can be seen in Table 2. For compounds with an adequate

Table 2. Effect of R<sup>1</sup>, R<sup>2</sup>, R<sup>3</sup>, and R<sup>4</sup> Substitutions of **4**



Cmpd	R <sup>1</sup>	R <sup>2</sup>	R <sup>3</sup>	R <sup>4</sup>	<sup>a</sup> SETD2 IC <sub>50</sub> (μM)	<sup>b</sup> ICW IC <sub>50</sub> (μM)
16	-H	H		-H	>200	
17	-H		-H	-H	0.818	2.04
18	-F		-H	-H	0.101	0.397
19	-F		-H	-H	0.066	0.54
20	-F		-H	-H	0.018	0.235
21	-F		-H	Me	0.017	0.379
22	-F		-H	-Cl	0.008	0.384
23	-F		-H	-F	0.003	0.175
24	-F		-H	-H	0.012	0.093
25	-F		-H	-F	0.007	0.029

<sup>a</sup>Standard deviations range from 3% to 63% of the IC<sub>50</sub> values.

<sup>b</sup>Standard deviations range from 7% to 67% of the IC<sub>50</sub> values.

biochemical potency, we demonstrated the activity in a cellular context using an in-cell Western (ICW) cell biochemical assay in A549 cells by monitoring the H3K36 trimethyl mark. We began by surveying the impact of the *meta*-substitution on the arene, as it had a notably improved activity over that of an exemplary analog with an *ortho*-substitution. The morpholine analog **17** had a submicromolar activity and, when combined with the C4 fluoride substitution on the indole core, the biochemical potency for **18** increased sixfold. Further investigation of the amine *meta*-substituent led to **20**, which had a fivefold increase in its biochemical potency over that of **18**. Next, we focused on the addition of a second *meta*-substituent, which was observed to further improve the biochemical potency in some cases, as seen in compounds **21**–**23**.

The translation of the biochemical activity into a cellular assay continued to prove challenging at this stage. We noted that many of the more biochemically potent compounds contained amines that would be expected to be quite basic and that compounds **22** and **23** in general displayed a large shift between the biochemical and cell biochemical assays. Several factors might explain such a shift, including the impact of basicity on the partition between

cellular compartments<sup>17</sup> and the effect of serum binding in the assay medium. To probe this hypothesis, we prepared nonbasic pyrrolidine analogs with an amide substituent. This effort furnished **24** and **25** with overall lower shifts between the biochemical and cellular assays, with **25** displaying a low-nanomolar potency in the cell biochemical assay.

During these studies, we were able to obtain an X-ray structure for **20** of the ligand-bound complex, as shown in Figure 3. The positioning of the indole ring is comparable to that in the

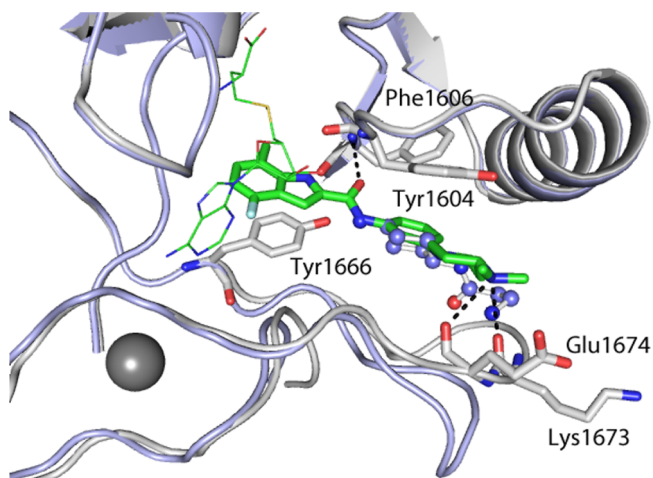


Figure 3. X-ray structure of **20** overlaid with **2**. Compound **20** is shown as green sticks, and compound **2** is shown as a ball and stick representation. The protein structures in the **20** and **2** costructures are shown in gray and blue, respectively.

structure for compound **2**, with similar  $\pi$ -stacking and hydrogen bonding interactions. The central aromatic ring of **20** makes  $\pi$ -stacking contacts with Tyr1604, and the *N*-aminopiperidine substituent points out toward the solvent. The steric disposition of the *N*-aminopiperidine in this structure was consistent with the observation that *meta*-substituents on the central aryl ring had higher cellular activities.

While **25** provided many key features that were desirable for an *in vivo* tool compound, there were a few additional areas to optimize. Analogs in Table 2 displayed a high lipophilicity and aromatic character; as a result, low aqueous solubilities were observed for several analogs, and low fractions absorbed were observed for those analogs we studied *in vivo*. The pharmacokinetic (PK) behavior of compound **25** in mice is shown in Table 3 as an example of this. While compound **25** shows a moderate clearance, we did not pursue *in vivo* studies, in part due to the low fraction absorbed (*Fa*).

To address this, we investigated the impact of alternatives to the compounds' central aromatic core using a saturated system similar to those of our original HTS hits **1** and **2**.<sup>18,19</sup> The resulting compounds (Table 4) displayed activities that were highly stereoselective, favoring the (1*R*,3*S*)-isomer. The activity generally tracked with those found in the corresponding aromatic series of compounds. Thus, merging those lessons from our SAR studies as outlined above, the optimal activity was found in aminopyrrolidine compounds such as **30** and **32**. This scaffold displayed much more favorable physical chemical, and ADME properties when compared to those of the analogous compounds with an aryl core. Additionally, the ADME properties measured *in vitro* generally translated well into *in vivo* PK. We chose to focus on compound **32** as it showed high

Table 3. Detailed Profile Assessments for 25 and 32

compound	25	32
hepatocyte $CL_{int}$ human/mouse (mL/min/kg)	64/239	51/721
Caco-2 $P_{appA-B}$ ( $10^{-6}$ cm/s), efflux ratio		3.2, 5.6
PSA ( $\text{\AA}^2$ )	68	87
cLogD	3.2	0.32
CYP 450 1A2, 2B6, 2C8, 2C9, 2C19, 2D6, and 3A4 inhibition, $IC_{50}$ ( $\mu\text{M}$ ) <sup>a</sup>		>50, >50, 16, 36, >50, >50, >50, >50
hERG $IC_{50}$ ( $\mu\text{M}$ )		4.5
PK parameters (mouse)		
CL (mL/min/kg)	24.2	53.3
$V_{ss}$ (L/kg)	1.04	8.13
terminal $t_{1/2}$ (h)	0.7	3.13
estimated $F_a$	<0.01 (50 mpk)	0.7 (30 mpk)
time over ICW $IC_{50}$ (h)	0 (50 mpk)	~6 (30 mpk), ~12 (100 mpk)

<sup>a</sup>Values are estimated  $IC_{50}$  values based on the percent (%) inhibition at a single concentration (50  $\mu\text{M}$ ).

potencies in both the biochemical and cell biochemical assays. We determined the  $K_i$  value for 32 to be 3.3 nM with an uncompetitive mechanism versus SAM and a noncompetitive mechanism versus the peptide (Supporting Information Figure 1). Although it displayed a relatively high intrinsic clearance *in vitro* in mouse hepatocytes, we reasoned that its decreased aromatic character might provide some benefits in oral absorption. The results for mouse PK studies for compound 32 are shown in Table 3. We found that compound 32 had a much higher oral absorption in mice as compared to that of

compound 25. Although 32 exhibited a relatively high *in vivo* clearance, the fraction absorbed at 10 mpk was estimated to be 0.6, indicating that 32 was well absorbed in a conventional formulation (0.5% CMC/0.1% Tween80), which can be attributed to its improved solubility and dissolution. Gratifyingly, oral exposure increased greater than dose-proportional as doses increased up to 100 mpk, thus providing sufficient exposure relative to the ICW  $IC_{50}$  for the use of compound 32 as a SETD2-inhibitory tool compound. Furthermore, 32 displayed a >8000-fold selectivity in a panel of 14 other histone methyltransferases, showing a remarkable level of selectivity over these closely related and potentially confounding targets. It showed minimal activity in a panel of 47 common off-target receptors and enzymes, showing only modest micromolar activity against three GPCRs. Finally, the compound showed no activity greater than 30% inhibition at 10  $\mu\text{M}$  in a panel of 45 kinases (see the Supporting Information)

Again, we confirmed the binding of 32 by cocrystallization, as shown in Figure 4. Like earlier analogs, the position of the indole was conserved, and the same contacts that were observed previously were seen here as well. The cyclohexane ring appears to make nonpolar contacts and principally serves to orient the pyrrolidine substituent in an appropriate direction toward the solvent. While the conformation of the ligand is well-defined by the electron density, the amino acid side chains of the protein loop proximal to the pyrrolidine sulfonamide (Lys1673 and Glu1674) are poorly defined, presumably reflecting the flexible nature of this region. As a result, no specific interactions between this portion of the ligand and the protein, either directly or via bound waters, were observed.

Compounds 32 and 33 were studied for their effects on the proliferation of two multiple myeloma cell lines, KMS34 and

Table 4. Structure–Activity Relationship of the 1,3-*cis*-Diaminocyclohexyl Substitution

Compound	R	<sup>a</sup> SETD2 $IC_{50}$ ( $\mu\text{M}$ )	<sup>b</sup> ICW $IC_{50}$ ( $\mu\text{M}$ )	$CL_{int}$ human (mL/min/kg)	$CL_{int}$ mouse (mL/min/kg)
26		0.147	0.449	75.0	2170
27		0.012	0.257	32.3	399
28		0.118	0.34	23.7	164
29		0.056	0.162	41	328
30		0.015	0.074	22.5	25.7
31		0.023	0.127	16.0	54.1
32		0.008	0.023	51	721
33		0.012	0.064	21.1	235

<sup>a</sup>Standard deviations range from 3% to 48% of the  $IC_{50}$  values. <sup>b</sup>Standard deviations range from 0.5% to 57% of the  $IC_{50}$  values.

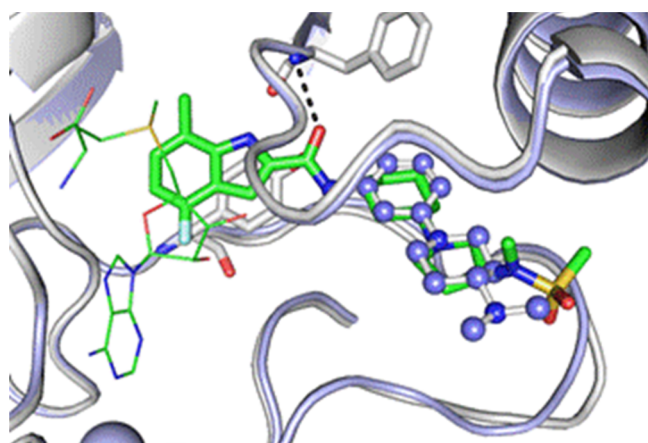


**Figure 4.** X-ray structure of **32** overlaid with **20**. Compound **32** is shown as green sticks, and compound **20** is shown as a ball and stick representation. The protein structures in the **32** and **20** costructures are shown in gray and blue, respectively.

KMS11, and the data can be seen in Table 5. The potent antiproliferative activity of compound **32** coupled with its

**Table 5. Anti-Proliferation Data of Relevant Cell Lines for **32** and **33** in 14 Day Long-Term Proliferation (LTP) Assays**

compound	KMS34 LTP day 14 IC <sub>50</sub> (μM)	KMS11 LTP day 14 IC <sub>50</sub> (μM)
<b>32</b>	0.025	0.211
<b>33</b>	0.038	0.476

encouraging PK behavior in mice suggested that it might prove suitable for study in appropriate xenograft models.<sup>20</sup>

Compound **32** and its related analogs disclosed in Table 4 can be prepared as outlined in Scheme 1 (analogous from Tables 1 and 2, see the Supporting Information). The synthesis begins with the condensation of hydrazine **34** with ethyl pyruvate, followed by a cyclic [3,3]-sigmatropic rearrangement and subsequent ammonium elimination in the presence of *p*-TsOH via a Fischer indole cyclization protocol. Basic saponification afforded the carboxylic acid **36** in a high yield. The installation of the amine partner was accomplished by a HATU-mediated

coupling with (1*R*,3*R*)-3-aminocyclohexan-1-ol, followed by a mild oxidation of the alcohol to the cyclohexanone **37**. Then, condensation of the secondary amine partner with **37** and a subsequent *in situ* reduction give a mixture of diastereomers (2:1 *cis/trans*). Finally, isolation by prep-HPLC chromatography completes the synthesis for EPZ-719 (**32**).

In summary, we began a campaign to identify an appropriate compound that could be used to interrogate SETD2 biology *in vivo*. A screen of our focused library directed toward epigenetic targets provided hit compounds **1** and **2**. **1** and **2** were modified in a sequential medicinal chemistry optimization process to lead to compound **32**, which met our goals for potency, selectivity, and ADME behavior suitable for *in vitro* and *in vivo* investigations of SETD2 biology. Structural insights gained from crystallographic studies served to elucidate the binding behavior of the inhibitors but proved limited in optimizing solvent-facing portions of the molecules due to the flexibility of the protein. Close attention to the physical chemical properties of the inhibitors, in particular basicity, lipophilicity, and aromatic character, led to compounds with attractive cellular activities and *in vivo* exposures. Additional results of *in vivo* studies on SETD2 biology and tumor growth inhibition in xenograft models are in preparation for a future manuscript.

## ■ ASSOCIATED CONTENT

### Supporting Information

The Supporting Information is available free of charge at <https://pubs.acs.org/doi/10.1021/acsmmedchemlett.1c00272>.

Synthetic procedures for all compounds; biochemical, cellular, ADME, and pharmacokinetic assay protocols; and crystallography protocols(PDF)

## ■ AUTHOR INFORMATION

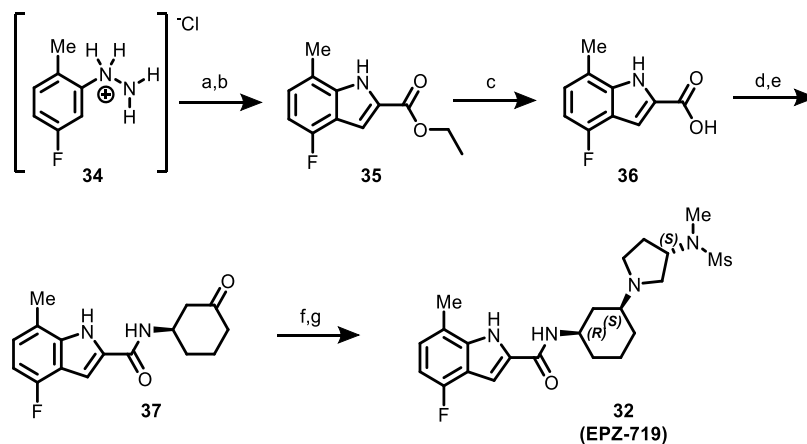
### Corresponding Author

Neil A. Farrow – Epizyme Inc., Cambridge, Massachusetts 02139, United States; [orcid.org/0000-0002-1469-0466](https://orcid.org/0000-0002-1469-0466); Email: [nfarrow@epizyme.com](mailto:nfarrow@epizyme.com)

### Authors

John W. Lampe – Epizyme Inc., Cambridge, Massachusetts 02139, United States

## Scheme 1. Synthesis of EPZ-719<sup>a</sup>



<sup>a</sup>Reagents and conditions are as follows: (a) ethyl pyruvate, H<sub>2</sub>SO<sub>4</sub>, EtOH, 88%; (b) *p*-TsOH, toluene, 100 °C, 23%; (c) NaOH, THF, MeOH, water, rt, 81%; (d) (1*R*,3*R*)-3-aminocyclohexan-1-ol, HATU, diisopropylethylamine, DMF, rt, 76%; (e) PCC, EtOAc, rt, 48%; (f) (*S*)-*N*-methyl-*N*-(pyrrolidin-3-yl)methanesulfonamide, NaBH<sub>3</sub>CN, MeOH, rt, 52%; (g) prep-HPLC.

**Joshua S. Alford** – Epizyme Inc., Cambridge, Massachusetts 02139, United States  
**P. Ann Boriak-Sjodin** – Epizyme Inc., Cambridge, Massachusetts 02139, United States; Present Address: Accent Therapeutics, 65 Hayden Avenue, Lexington, Massachusetts 02421, United States  
**Dorothy Brach** – Epizyme Inc., Cambridge, Massachusetts 02139, United States  
**Kat Cosmopoulos** – Epizyme Inc., Cambridge, Massachusetts 02139, United States  
**Kenneth W. Duncan** – Epizyme Inc., Cambridge, Massachusetts 02139, United States; Present Address: Accent Therapeutics, 65 Hayden Avenue, Lexington, Massachusetts 02421, United States  
**Sean T. Eckley** – Epizyme Inc., Cambridge, Massachusetts 02139, United States  
**Megan A. Foley** – Epizyme Inc., Cambridge, Massachusetts 02139, United States; Present Address: Blueprint Medicines, 45 Sidney Street, Cambridge, Massachusetts 02139, United States.  
**Darren M. Harvey** – Epizyme Inc., Cambridge, Massachusetts 02139, United States; Present Address: 28-7 Therapeutics, 490 Arsenal Way, Suite 100B, Watertown, Massachusetts 02472, United States.  
**Vinny Motwani** – Epizyme Inc., Cambridge, Massachusetts 02139, United States  
**Michael J. Munchhof** – Epizyme Inc., Cambridge, Massachusetts 02139, United States; Present Address: Munchhof LLC, 335 Frost Lane, Corvallis, Montana 59828, United States.  
**Alejandra Raimondi** – Epizyme Inc., Cambridge, Massachusetts 02139, United States  
**Thomas V. Riera** – Epizyme Inc., Cambridge, Massachusetts 02139, United States  
**Cuyue Tang** – Epizyme Inc., Cambridge, Massachusetts 02139, United States; Present Address: Remix Therapeutics, One Kendall Square, Building 200, Cambridge, Massachusetts 02139, United States.  
**Michael J. Thomenius** – Epizyme Inc., Cambridge, Massachusetts 02139, United States; Present Address: Foghorn Therapeutics, 500 Technology Square, Suite 700, Cambridge, Massachusetts 02139, United States.  
**Jennifer Totman** – Epizyme Inc., Cambridge, Massachusetts 02139, United States

Complete contact information is available at:  
<https://pubs.acs.org/10.1021/acsmchemlett.1c00272>

### Author Contributions

The manuscript was written through contributions of all authors.

### Notes

The authors declare the following competing financial interest(s): All authors are/were employees of Epizyme, Inc. Work was funded by Epizyme.  
The coordinates of SETD2 in complex with **2**, **20**, and **32** have been deposited under PDB IDs 7LZB, 7LZD, and 7LZF, respectively.

### REFERENCES

(1) Sun, X. J.; Wei, J.; Wu, X. Y.; Hu, M.; Wang, L.; Wang, H. H.; Zhang, Q. H.; Chen, S. J.; Huang, Q. H.; Chen, Z. Identification and characterization of a novel human histone H3 lysine 36-specific methyltransferase. *J. Biol. Chem.* **2005**, *280* (42), 35261–71.

(2) Edmonds, J. W.; Mahadevan, L. C.; Clayton, A. L. Dynamic histone H3 methylation during gene induction: HYPB/Setd2 mediates all H3K36 trimethylation. *EMBO J.* **2008**, *27* (2), 406–20.

(3) Aymard, F.; Bugler, B.; Schmidt, C. K.; Guillou, E.; Caron, P.; Brioso, S.; Iacovoni, J. S.; Daburon, V.; Miller, K. M.; Jackson, S. P.; Legube, G. Transcriptionally active chromatin recruits homologous recombination at DNA double-strand breaks. *Nat. Struct. Mol. Biol.* **2014**, *21* (4), 366–74.

(4) Carvalho, S.; Vitor, A. C.; Sridhara, S. C.; Martins, F. B.; Raposo, A. C.; Desterro, J. M.; Ferreira, J.; de Almeida, S. F. SETD2 is required for DNA double-strand break repair and activation of the p53-mediated checkpoint. *eLife* **2014**, *3*, No. e02482.

(5) de Almeida, S. F.; Grosso, A. R.; Koch, F.; Fenouil, R.; Carvalho, S.; Andrade, J.; Levezinho, H.; Gut, M.; Eick, D.; Gut, I.; Andrau, J. C.; Ferrier, P.; Carmo-Fonseca, M. Splicing enhances recruitment of methyltransferase HYPB/Setd2 and methylation of histone H3 Lys36. *Nat. Struct. Mol. Biol.* **2011**, *18* (9), 977–83.

(6) Luco, R. F.; Pan, Q.; Tominaga, K.; Blencowe, B. J.; Pereira-Smith, O. M.; Misteli, T. Regulation of alternative splicing by histone modifications. *Science* **2010**, *327* (5968), 996–1000.

(7) Dalglish, G. L.; Furge, K.; Greenman, C.; Chen, L.; Bignell, G.; Butler, A.; Davies, H.; Edkins, S.; Hardy, C.; Latimer, C.; Teague, J.; Andrews, J.; Barthorpe, S.; Beare, D.; Buck, G.; Campbell, P. J.; Forbes, S.; Jia, M.; Jones, D.; Knott, H.; Kok, C. Y.; Lau, K. W.; Leroy, C.; Lin, M. L.; McBride, D. J.; Maddison, M.; Maguire, S.; McLay, K.; Menzies, A.; Mironenko, T.; Mulderrig, L.; Mudie, L.; O'Meara, S.; Pleasance, E.; Rajasingham, A.; Shepherd, R.; Smith, R.; Stebbings, L.; Stephens, P.; Tang, G.; Tarpey, P. S.; Turrell, K.; Dykema, K. J.; Khoo, S. K.; Petillo, D.; Wondereg, B.; Anema, J.; Kahnoski, R. J.; Teh, B. T.; Stratton, M. R.; Futreal, P. A. Systematic sequencing of renal carcinoma reveals inactivation of histone modifying genes. *Nature* **2010**, *463* (7279), 360–3.

(8) Duns, G.; van den Berg, E.; van Duivenbode, I.; Osinga, J.; Hollema, H.; Hofstra, R. M.; Kok, K. Histone methyltransferase gene SETD2 is a novel tumor suppressor gene in clear cell renal cell carcinoma. *Cancer Res.* **2010**, *70* (11), 4287–91.

(9) Fontebasso, A. M.; Schwartzentruber, J.; Khuong-Quang, D. A.; Liu, X. Y.; Sturm, D.; Korshunov, A.; Jones, D. T.; Witt, H.; Kool, M.; Albrecht, S.; Fleming, A.; Hadjadj, D.; Busche, S.; Lepage, P.; Montpetit, A.; Staffa, A.; Gerges, N.; Zakrzewska, M.; Zakrzewski, K.; Liberski, P. P.; Hauser, P.; Garami, M.; Klekner, A.; Bogner, L.; Zadeh, G.; Faury, D.; Pfister, S. M.; Jabado, N.; Majewski, J. Mutations in SETD2 and genes affecting histone H3K36 methylation target hemispheric high-grade gliomas. *Acta Neuropathol.* **2013**, *125* (5), 659–69.

(10) Hakimi, A. A.; Ostrovnaya, I.; Reva, B.; Schultz, N.; Chen, Y.-B.; Gonen, M.; Liu, H.; Takeda, S.; Voss, M. H.; Tickoo, S. K.; Reuter, V. E.; Russo, P.; Cheng, E. H.; Sander, C.; Motzer, R. J.; Hsieh, J. J. Adverse outcomes in clear cell renal cell carcinoma with mutations of 3p21 epigenetic regulators BAP1 and SETD2: a report by MSKCC and the KIRC TCGA research network. *Clin. Cancer Res.* **2013**, *19* (12), 3259–3267.

(11) Grassian, A. R.; Thomenius, M.; Totman, J. A. Methods of treating cancer by inhibiting SETD2. WO 2019/036466 A1, 2019.

(12) Zheng, W.; Ibanez, G.; Wu, H.; Blum, G.; Zeng, H.; Dong, A.; Li, F.; Hajian, T.; Allali-Hassani, A.; Amaya, M. F.; Siarheyeva, A.; Yu, W.; Brown, P. J.; Schapira, M.; Vedadi, M.; Min, J.; Luo, M. Sinefungin derivatives as inhibitors and structure probes of protein lysine methyltransferase SETD2. *J. Am. Chem. Soc.* **2012**, *134* (43), 18004–14.

(13) Mitchell, L. H.; Boriak-Sjodin, P. A.; Smith, S.; Thomenius, M.; Rioux, N.; Munchhof, M.; Mills, J. E.; Klaus, C.; Totman, J.; Riera, T. V.; Raimondi, A.; Jacques, S. L.; West, K.; Foley, M.; Waters, N. J.; Kuntz, K. W.; Wigle, T. J.; Scott, M. P.; Copeland, R. A.; Smith, J. J.; Chesworth, R. Novel Oxindole Sulfonamides and Sulfamides: EPZ031686, the First Orally Bioavailable Small Molecule SMYD3 Inhibitor. *ACS Med. Chem. Lett.* **2016**, *7* (2), 134–8.

(14) Blat, Y. Non-competitive inhibition by active site binders. *Chem. Biol. Drug Des.* **2010**, *75* (6), 535–40.

- (15) Drew, A. E.; Moradei, O.; Jacques, S. L.; Rioux, N.; Boriack-Sjodin, A. P.; Allain, C.; Scott, M. P.; Jin, L.; Raimondi, A.; Handler, J. L.; Ott, H. M.; Kruger, R. G.; McCabe, M. T.; Sneeringer, C.; Riera, T.; Shapiro, G.; Waters, N. J.; Mitchell, L. H.; Duncan, K. W.; Moyer, M. P.; Copeland, R. A.; Smith, J.; Chesworth, R.; Ribich, S. A. Identification of a CARM1 Inhibitor with Potent In Vitro and In Vivo Activity in Preclinical Models of Multiple Myeloma. *Sci. Rep.* **2017**, *7* (1), 17993.
- (16) Mitchell, L. H.; Drew, A. E.; Ribich, S. A.; Rioux, N.; Swinger, K. K.; Jacques, S. L.; Lingaraj, T.; Boriack-Sjodin, P. A.; Waters, N. J.; Wigle, T. J.; Moradei, O.; Jin, L.; Riera, T.; Porter-Scott, M.; Moyer, M. P.; Smith, J. J.; Chesworth, R.; Copeland, R. A. Aryl Pyrazoles as Potent Inhibitors of Arginine Methyltransferases: Identification of the First PRMT6 Tool Compound. *ACS Med. Chem. Lett.* **2015**, *6* (6), 655–9.
- (17) Black, W. C.; Percival, M. D. The consequences of lysosomotropism on the design of selective cathepsin K inhibitors. *ChemBioChem* **2006**, *7* (10), 1525–35.
- (18) Ritchie, T. J.; Macdonald, S. J.; Peace, S.; Pickett, S. D.; Luscombe, C. N. Increasing small molecule drug developability in sub-optimal chemical space. *MedChemComm* **2013**, *4* (4), 673–680.
- (19) Ritchie, T. J.; Macdonald, S. J.; Young, R. J.; Pickett, S. D. The impact of aromatic ring count on compound developability: further insights by examining carbo- and hetero-aromatic and -aliphatic ring types. *Drug Discovery Today* **2011**, *16* (3–4), 164–71.
- (20) SETD2 target engagement for **32** and related compounds was confirmed via a direct correlation between the reduction of H3K36me3 levels and *in vitro* cellular antiproliferative effects. These data were presented by Totman et al. at EHA 2021 (HemaSphere 2021, 5:S2, 44) and will be detailed in a SETD2 biology-focused manuscript in preparation.